Tellus (1992), *44A*, 331–338

Predictability of the zonal index in a global model

By WALTER A. ROBINSON AND JIANCHUN QIN, *Department of Atmospheric Sciences, University of Illinois at Urbana-Champaign, 105 South Gregory Avenue, Urbana, Illinois 61801, USA*

(Manuscript received 30 October 1991; in final form 9 March 1992)

ABSTRACT

Using the model twin formulation, the predictability of the zonal index, an inherently low-frequency feature of the circulation, is studied in a two-layer, global, zonally homogeneous model. While typical periods for variability in the zonal index are on the order of 100 days, the index is predictable with useful skill only out to 23 days. The predictability of the zonal index shares some behavior with the predictability of time averages. A simple model of the growth of forecast error in the zonal index is constructed. The model demonstrates that the combination of a long timescale with relatively poor predictability is consistent with the behavior of a feature that acts as a dynamical filter of synoptic scale noise.

1. Introduction

In the atmosphere, low-frequency variability arises from slow changes in boundary conditions and from the nonlinearity of the internal dynamics. While the relative importance of internal dynamics and external forcing in determining low-frequency behavior is unknown, there is growing evidence that internal dynamics can, by itself, generate robust low-frequency variability (Cai and van den Dool, 1991; Cai and Mak, 1990; Mo et al., 1991; Qin and Robinson, 1992; Robinson, 1991a, b). Long-range forecasting, therefore, depends on knowing the present state and being able to predict the future state of the lower boundary (e.g., sea-surface temperatures), but also on the ability to predict the evolution of slow variations generated by internal dynamics.

In the present paper we examine the predictability of one of the dominant modes of low-frequency variability in a simple nonlinear model of the atmosphere. This feature, the zonal index (*ZI*), is of interest for several reasons. First, it is an inherently low-frequency phenomenon; no temporal filtering is required to reveal its low-frequency behavior. Secondly, the zonal index is the dominant mode determining the character of middle-latitude "weather" in our model. And thirdly, the zonal index in our model is very similar to important zonally symmetric modes of variability that have recently been found in general circulation models (Branstator, 1990), and in observations (Kidson, 1985; 1986; 1988; Karoly, 1990). The predictability of the zonal index, and consequently of stationary middle-latitude planetary waves, was investigated by Tung and Rosenthal (1986) in the context of a quasi-geostrophic channel model. Their results will be compared with those from the present study in the final section of this paper.

The model and the calculation of the zonal index are described by Robinson (1991b). Briefly, the model is a two-layer, global, primitive equation model, with zonally homogeneous boundary conditions. It is a spectral model, run at rhomboidal 15 spherical harmonic truncation, with thermal forcing appropriate to the Northern Hemisphere winter.

The zonal index is the leading empirical orthogonal function of the Northern Hemisphere zonally and vertically averaged angular momentum. A high value of *ZI* corresponds to a northward displacement of the subtropical jet from its mean latitude, and visa versa. In this respect *ZI* is similar to traditional measures of the zonal index. The spectrum of the zonal index is very red for periods less than 100 days. Fig. 1 shows the logarithmic spectrum (Zangvil, 1981) of the zonal index determined from the final 5120 days of a 6000 day run of the model. The

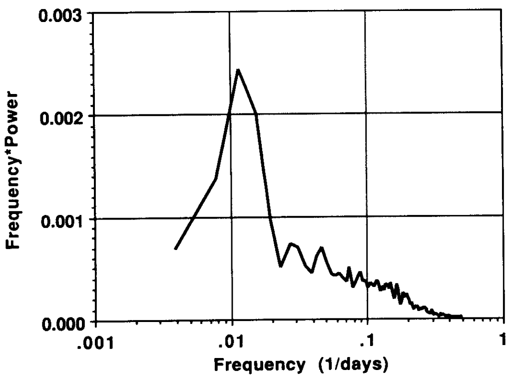

Fig. 1. Logarithmic spectrum of the variability of the zonal index in a 6000 day run of the two-layer model.

spectrum is calculated by dividing the record into 20 segments of 256 days. Each segment is Hanning windowed, and the spectrum is determined by a fast fourier transform. The spectrum displayed is the average of the 20 spectra. It has a sharp peak around a period of 100 days, and there is very little power at periods shorter than 50 days.

The approach taken to determine the predictability of *ZI* employs the "model twin" formulation (Tribbia and Baumhefner, 1988). The design of these experiments and their results are discussed in Section 2. Section 3 describes a simple analytic model for the loss of predictability in *ZI*, and the final section is a summary of the results with a discussion of their implications.

2. Predictability experiments

The predictability of *ZI* in our two-layer model is determined from 60 twin experiments: 36 of 60 days duration and 24 of 100 days duration. Each pair of twins includes a control run and a perturbed run. The initial condition for each control is selected at random from the first 3000 days of the 6000-day model run. The initial condition for each perturbed run is identical to that of its twin except that a small perturbation is added to the model field. This perturbation is obtained by taking the 10-day high-pass filtered fields from another randomly chosen day and multiplying them by a small number, 0.01. The 10-day high pass fields are in turn calculated by subtracting the 10-day low-pass filtered data (Blackmon, 1976) from the full model output.

The results for the 60 twins are shown in Fig. 2 in terms of root mean square (rms) forecast error and the anomaly correlation. The former quantity is given by,

$$\delta ZI^{\mathrm{rms}}(t) = \langle (ZI^{\mathrm{control}}(t) - ZI^{\mathrm{perturbed}}(t))^2 \rangle^{1/2}, \tag{2.1}$$

and the anomaly correlation is given by,

$$C(t) = \frac{\langle \Delta ZI^{\mathrm{control}}(t) \times \Delta ZI^{\mathrm{perturbed}}(t) \rangle}{\langle \Delta ZI^{\mathrm{control}}(t)^2 \, \Delta ZI^{\mathrm{perturbed}}(t)^2 \rangle^{1/2}}, \tag{2.2}$$

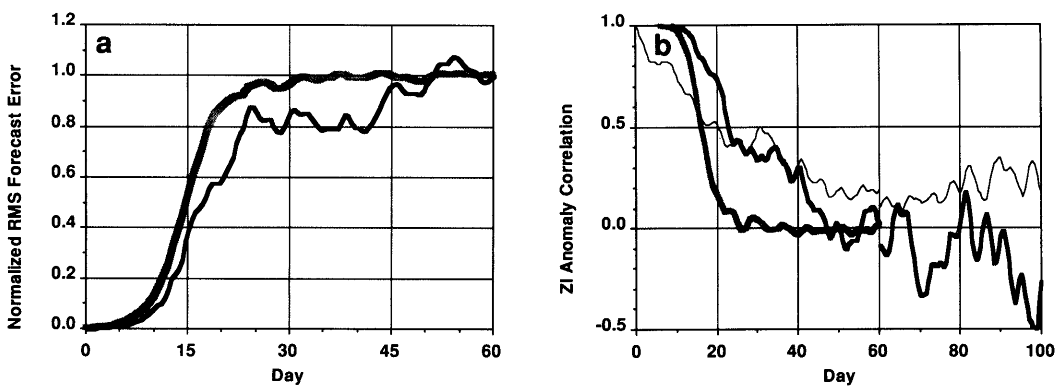

Fig. 2. (a) Normalized rms forecast errors from 60 model twin experiments for the zonal index (solid curve), and the 500 mb streamfunction (thick shaded curve). (b) Anomaly correlations between *ZI* in the forecast and control model twins (heavy solid curve), anomaly correlations between *ZI* in the control and its value at day 0 (thin solid curve), and anomaly correlations between forecast and control 500 mb streamfunction fields (thick shaded curve). The curves for the model twin and persistence forecasts of *ZI* break at day 60. At earlier times they are based on 60 experiments, while after day 60 they are based on only 24 experiments.

where the brackets indicate an ensemble average,

$$\langle X \rangle = \frac{1}{60} \sum_{i=1}^{60} X_i, \tag{2.3}$$

and the anomaly in ZI, ΔZI, is given by,

$$\Delta ZI = ZI - \overline{ZI}, \tag{2.4}$$

where $\overline{ZI}$ is the climatological mean of ZI calculated from the final 5980 days of the 6000 model run. For both quantities the corresponding curves are also shown for the barotropic component (500 mb value) of the Northern Hemisphere streamfunction. The rms errors are normalized by their mean values over the final 15 days of the experiments, and the anomaly correlations for the 500 mb streamfunction are the average of the pattern correlations between the deviations from climatology of the streamfunction in the perturbed and control runs.

Both panels in Fig. 2 suggest that the zonal index is significantly more predictable in our model than the overall barotropic flow. What is perhaps surprising, however, is that ZI becomes unpredictable by the twin forecasts in such a short time. If an anomaly correlation of 0.5 is used to define the limit of useful forecasting, then ZI is predictable for about 23 days. Furthermore, it is seen that the predictability of ZI lasts for only a week beyond that of the 500 mb flow, and that ZI loses predictability on a much shorter timescale than its typical periods, which, according to its spectrum, are close to 100 days.

Our estimate of 16 days for the predictability of the 500 mb streamfunction is generous compared with that of other studies. Tribbia and Baumhefner, for example, found that anomaly correlations at 500 mb dropped below 0.5 in 10 days. Part of this difference may be explained by the small initial errors used in this study, an initial rms error at 500 mb of 0.7 m compared with the 1.5 m initial errors used by Tribbia and Baumhefner. It takes 2.5 days for errors in the present model to reach 1.5 m, so even after correcting for the smaller initial perturbation, our model loses predictability at 500 mb significantly more slowly than the model they used, the Community Climate Model (CCM). A possible explanation for this discrepancy is that initial errors for the present model are taken from its synoptic timescale variability, and are, therefore, not truly random. Also, there is no convection in our model, and convection may contribute to the more rapid growth of errors in the CCM.

The long timescales present in the variability of ZI suggest that persistence may be a useful forecast at some ranges. Fig. 2 also shows anomaly correlations for persistence forecasts. Simple persistence, i.e., the day 0 value of ZI, is an as good or better forecast than the model twin for all ranges greater than 25 days. At ranges of greater than 50 days the anomaly correlations of the twin forecasts fluctuate about zero, while anomaly correlations for persistence level off at a value between 0.1 and 0.2. While it is unlikely that such low anomaly correlations could be of any practical use, it is not clear why this persistence is lost in the twins.

A similar result is found in forecasts for the monthly averages of ZI (Table 1). For the average of ZI over the first 30 days, the model twin provides the best forecast, though persistence would explain about half of the variance in the 60 runs. For the average of ZI over the second month, the best forecast is the average of the twin forecast over the *first* month, followed by persistence from day 0, and the worst forecast is the average of the model twin forecast over the second month.

The importance of persistence can be seen in the forecasts for the daily values of ZI, as well as in the monthly means. Fig. 3 shows the day of the twin run that has the largest anomaly correlation with ZI in the control, across the 60 pairs of runs. Also shown is the value of that "best" anomaly correlation. The model twins provide useful forecast information only for the first two weeks. At later times the best forecast is to assume persistence from the day 14 or 15 twin forecast. Using this strategy, the maximum range for useful forecasts of ZI (anomaly correlations greater than 0.5) is

Table 1. *Anomaly correlations for the monthly mean zonal index; correlations are with the monthly means of the first and second months of the twins and with a persistence forecast*

Forecast Type	Month 1	Month 2
twin (month 1)	0.89	0.41
twin (month 2)	0.41	0.16
persistence (day 0)	0.71	0.30

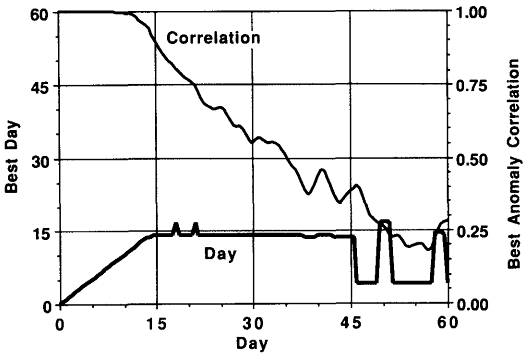

Fig. 3. Highest anomaly correlation between ZI and the model twins at all forecast days and the forecast day that gives this highest correlation.

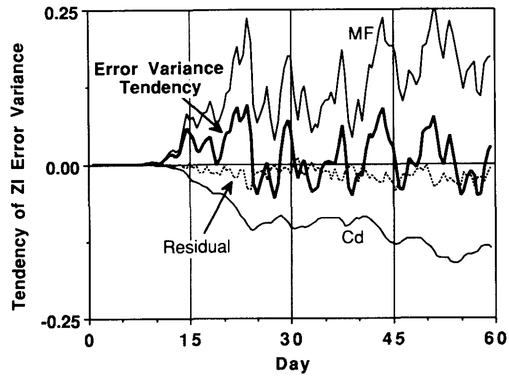

Fig. 4. Terms in the equation for the evolution of the variance of the forecast error for ZI.

extended to 35 days. This result, that all the useful information for forecasting ZI at the extended range comes from early in the model integration, is similar to Roads' (1987a, b) result for time averaged forecasts. A possible inference from this similarity is that ZI acts like a temporal average of the behavior of the two-layer model. We return to this point in the next section.

The growth of forecast errors in ZI can be diagnosed using the equation for the evolution of the index. Following Robinson (1991b), this equation is,

$$\frac{\mathrm{d}(\delta ZI)}{\mathrm{d}t} = \delta MF - C_\mathrm{d}\,\delta ZI + \delta Res, \tag{2.5}$$

where for any quantity, X, its forecast error, δX, is given by,

$$\delta X = X^{\text{perturbed}} - X^{\text{control}} \tag{2.6}$$

The terms on the r.h.s. of (2.5) are the forcing of the index by the transient flux of momentum, the effect of surface drag, and a residual that includes the effects of diffusive dissipation on the index and whatever errors are introduced in the calculation of the other terms. An equation for the growth of error variance, over the ensemble of experiments, is obtained by multiplying (2.5) by δZI for each pair of twins and taking the ensemble average;

$$\frac{\mathrm{d}\langle \delta Z^2 \rangle}{\mathrm{d}t} = 2\langle \delta MF\,\delta ZI \rangle - 2C_\mathrm{d}\langle \delta Z^2 \rangle + 2\langle \delta Res\,\delta ZI \rangle. \tag{2.7}$$

Fig. 4 shows the evolution of the three terms on the r.h.s. of (2.7) that contribute to the evolution of the error variance of ZI. The growth in error in the forecast of ZI is driven by errors in forecasting the eddy momentum fluxes. Once the errors in ZI are sufficiently large, around day 25, drag limits further growth, and the tendency of the error variance fluctuates about zero. The contribution from Res is small, and, because it includes the effect of diffusion, it tends to be negative.

3. A simple model for the growth of forecast errors

The simplest possible model of the growth in errors in model twin forecasts of ZI is to assume a one-way interaction with essentially random forcing by the eddies through their momentum fluxes. In this case the error in the forecast of ZI would obey a simple equation of the form,

$$\frac{\mathrm{d}(\delta ZI)}{\mathrm{d}t} = \varepsilon - C_\mathrm{d}\,\delta ZI, \tag{3.1}$$

where ε is some randomly varying function of time that represents the forcing of error growth by errors in the eddies. The variance of ε would be expected to grow from initially small values to some saturation value on a timescale similar to that of the overall growth of errors in the model. It remains to be seen whether such a simple model is consistent with the behavior of the two-layer model. After the initial period of transient error growth the twins should be uncorrelated, and the statistics of δZI should become identical to those of ΔZI. Eq. (3.1) predicts that the logarithmic spectrum of δZI will have a maximum at a frequency, $f_{\max}$, given by,

$$f_{\max} = \frac{C_d}{2\pi}. \tag{3.2}$$

For $C_d = 0.1$ days^{-1}, $f_{\max} = 0.016$ days^{-1}, which is somewhat greater than the frequency at the peak in Fig. 1.

Equation (3.1) can be made more general by including a positive feedback between the zonal index and its forcing by the momentum flux, i.e.,

$$\delta MF = \varepsilon + \alpha\, \delta ZI. \tag{3.3}$$

The strong positive correlations between the zonal index and its forcing by synoptic eddies found by Robinson (1991b) suggests that such a feedback may be present in the two-layer model. Adding a positive feedback to (3.1) it becomes,

$$\frac{d(\delta ZI)}{dt} = \varepsilon - (C_d - \alpha)\, \delta ZI. \tag{3.4}$$

In order to determine the predictability of index errors obeying eq. (3.4), some assumptions must be made regarding the temporal behavior of the random forcing, ε. We assume that ε is piecewise constant in time, but at a random value with a variance that increases from zero initially to a saturation value, i.e.,

$$\varepsilon(t) = A_i R_i, \qquad i\tau \leqslant t \leqslant (i+1)\tau, \quad i = 0, 1, 2, \ldots, \tag{3.5}$$

where R_i is a random number with unit variance, and A_i represents the increase in error variance with time,

$$A_i = \begin{cases} \frac{1}{4}\left[1 - \cos\left(\frac{i\pi\tau}{T}\right)\right]^2, & i\tau \leqslant T \\ 1, & i\tau > T \end{cases}. \tag{3.6}$$

The solution of (3.4), if the initial error is zero, is

$$\delta ZI(t) = \int_0^t \varepsilon(t')\, e^{-\beta(t-t')}\, dt', \tag{3.7}$$

where $\beta = C_d - \alpha$. Substituting from (3.5) yields,

$$\delta ZI(j\tau) = \frac{e^{-j\beta\tau}(1 - e^{-\beta\tau})}{\beta} \sum_{i=1}^{j} A_i R_i e^{i\beta\tau}. \tag{3.8}$$

The error variance at time $t = j\tau$, is then given by,

$$\langle \delta ZI(j\tau)^2 \rangle \approx \tau^2 e^{-2j\beta\tau} \sum_{i=1}^{j} A_i^2 e^{2i\beta\tau}, \tag{3.9}$$

for $\beta\tau \ll 1$. The error variance in the momentum flux is given by,

$$\langle \delta MF^2 \rangle = \alpha^2 \langle \delta ZI^2 \rangle + A_j^2. \tag{3.10}$$

At long times, $t \to \infty$, these quantities take on the values,

$$\langle \delta ZI^2 \rangle = \frac{\tau}{2\beta}, \qquad \langle \delta MF^2 \rangle = 1 + \frac{\alpha^2\tau}{2\beta}. \tag{3.11}$$

For values of the parameters that are relevant to ZI in the two-layer model, $\alpha^2\tau/2\beta \ll 1$, and the ratio of the variance of the errors in ZI to those in MF, as $t \to \infty$, is approximately given by,

$$R \equiv \left[\frac{\langle \delta ZI^2 \rangle}{\langle \delta MF^2 \rangle}\right]_{t \to \infty} = \frac{\tau}{2\beta}. \tag{3.12}$$

In order to match the saturation error variances of MF and ZI in the two level model, R can be estimated from the model results, and α and τ must satisfy,

$$\tau = 2R(C_d - \alpha). \tag{3.13}$$

From the final 30 days of the 24, 100-day twins, an average value for R is 12.7 days^2. Our model for error growth, (3.9), can then generate a family of curves for the growth of rms errors or the decay in forecast anomaly correlations, for different values of the feedback parameter, α. (The anomaly correlations are simply the square of the rms errors subtracted from 1.) For each value of α, the associated value for the forcing timescale, τ, is given by (3.13). These curves are shown in Fig. 5, with the appropriate results from the model twins shown for comparison. The curves in Fig. 5 are

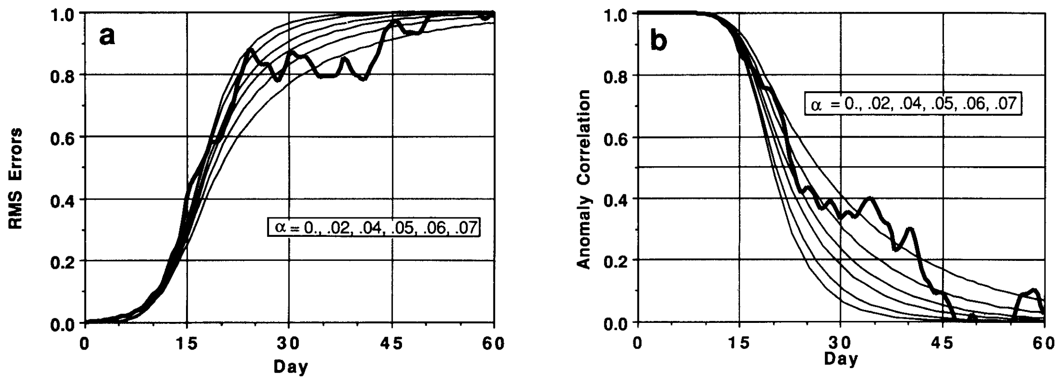

Fig. 5. Rms error in *ZI* from the 60 model twins compared with the error growth in the simple model. The simple model uses a time $T = 20$ days for the growth of random errors, and curves are shown for different values of the feedback parameter, α. Starting from the top, $\alpha = 0$, 0.02, 0.04, 0.05, 0.06, 0.07. (b) As in (a), except for the *ZI* anomaly correlation.

generated assuming a 20 day turn-on time, *T*, for the amplitude of the random errors.

As is clear from Fig. 5, the simple model does not do especially well in simulating the detailed temporal growth of forcast errors in *ZI* in the model twins. The simple' model is successful, however, in showing how an atmospheric feature that acts as a dynamical filter of synoptic "noise" can exhibit both a red spectrum and a rapid loss of predictability. From Fig. 5 it appears that 0.05 days^{-1} is a reasonable value for α ($\tau =$ 1.3 days). For this value the anomaly correlation falls below 0.5 in 25 days, but the spectrum of δZI peaks at a frequency of 0.008 days^{-1} (a period of 126 days).

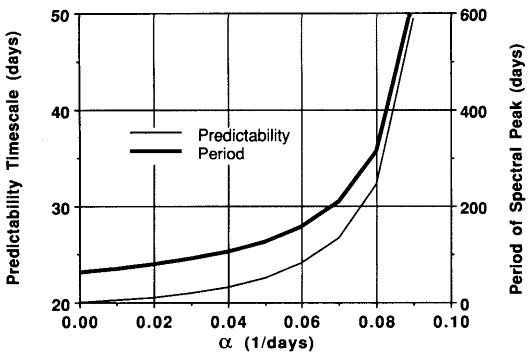

Fig. 6. Predictability, defined as the time at which the anomaly correlation drops to 0.5, and the characteristic period of variations, in the simple model, as a function of the feedback parameter, α.

The mismatch between the characteristic time-scale of variations in *ZI* and its predictability is insensitive to the strength of the positive feedback. Fig. 6 shows the predictability (the time at which the anomaly correlation decays to 0.5) and the period of the spectral peak for *ZI* as a function of the feedback parameter, α. As the feedback cancels more and more of the effect of dissipation, the periods and predictability increase, but the period remains about a factor of 10 longer than the predictability. As α increases, however, the amount of variability in *ZI* to be forecast increases according to (3.11).

4. Summary and discussion

Our principal finding is that an inherently low-frequency feature of the dynamical variability in a nonlinear model can be effectively forecast over times that are much shorter than the characteristic period of the variability. The zonal index, *ZI*, in our two-layer model has its strongest variability at periods close to 100 days, but it can be forecast by model twins with useful skill only about 25 days in advance.

The predictability of *ZI* is reminiscent of the predictability of time-averages, studied by Roads (1987a, b), suggesting that variability in *ZI* represents dynamically filtered variability in the synoptic eddies. In particular, a forecaster living in our model would derive no benefit, in terms of forecasting ZI, from running a numerical forecasting model for more than two weeks.

Comparing the results with those from a simple model of the error growth suggests that both the long timescales present in timeseries of ZI and its predictability are in part due to the existence of a positive feedback between the zonal index and its forcing by eddy momentum fluxes. The greater the strength of such a feedback, the longer will be the characteristic periods of fluctuations in ZI, and the greater will be its predictability. A value of about 0.05 days^{-1} for the feedback parameter appears to produce the best match between the simple model and our forecasting experiments. At this value the feedback cancels half of the dissipative effect of surface drag.

The physical mechanism of the positive feedback remains, however, somewhat uncertain. The strongest candidate involves the modulation by the zonal index of the generation of eddy activity by baroclinic instability. First, Robinson (1991b) noted that the baroclinic component of the jet followed the meridional displacements in its barotropic component that are associated with variations in ZI. Secondly, baroclinic instability calculations, conducted with basic states with a range of values of ZI, show that the most unstable wave, wavenumber 7, has maxima in its amplitude at two latitudes: in the subtropics and in higher latitudes. The high-latitude maximum is stronger for basic states with larger ZI. Hence, the average latitude at which eddy activity is generated follows the meridional excursions of the jet under variations in ZI, at least to the extent that the linear most unstable modes are relevant to the nonlinear model. If the effect of the eddies over a baroclinic lifecycle is to converge momentum into the region of initial generation, then the meridional shift in the baroclinically unstable waves with changes in ZI will lead to a positive feedback.

Such a mechanism might also explain some of the marked differences between the behaviors of the two-layer model and the simple model. In particular, a positive feedback that depends on the behavior of eddies over an entire baroclinic life cycle could be most effective in amplifying (or opposing the dissipation of) variations in ZI on longer timescales. Replacing our frequency independent feedback with one that worked preferentially for low frequencies could correct the principal deficiency of our simple model, that it overestimates the growth of forecast errors at times greater than a month. Statistical techniques exist that would permit the construction of a model for the feedback that would be optimal in terms of reproducing the behavior of the model twins. It is not clear, however, that this approach would contribute significantly to our understanding.

A final point is how the present results relate to those of Tung and Rosenthal (1986), who considered the predictability of the zonal index in a quasi-geostrophic channel model with orography. A detailed comparison is difficult, because there is no orography in our model, and because they treated as fixed the sole quantity responsible for the loss of predictability in our model, the zonally averaged momentum fluxes by transient eddies. Nothing in the present results, however, contradicts their finding that the zonal index is predictable for at least 10 days.

A key finding of Tung and Rosenthal was that orographic form drag is unlikely to be an important mechanism for the growth of forecast errors, for reasonable settings of the parameters. While the model discussed above cannot address the issue of orographic forcing, we have also run our model with orography, an isolated mountain centered at 40° N. The orography is included as described by Hendon (1986). As in the present case, the model with orography has a dominant mode of zonally symmetric variability that is used to define the zonal index, and the spectrum of its variability is very similar to that in the zonally homogeneous model. The index EOF has a node at the same latitude as the center of the mountain. This prevents orographic form drag from having a significant influence on the evolution of the index. The index does, however, influence the orographic stationary waves. These waves are substantially different in high and low index states, and the stationary eddy field is most persistent where the orographic eddies are most affected by the difference between high and low index zonal flows.

The results of our experiments with an isolated mountain are, therefore, consistent with those of Tung and Rosenthal in two respects. First, variations in the zonal index, through their interaction with the orography, are an important source of the variations in the low-frequency eddies, and secondly, the orographic form drag does not contribute significantly to the evolution of the index. The strong feedback between the stationary waves and the zonal flow, by way of the mountain torque, that is required for form drag instability, is not present, and, therefore, form-drag instability cannot contribute significantly to the growth of forecast errors. It is possible that given a different orography, a meridionally elongated ridge for example, the orographic form drag might interact with the zonal flow in such a way as the enhance the predictability of the index beyond that found in the present work, thereby improving the predictability of the orographic stationary waves (K. K. Tung, personal communication). We plan to carry out experiments with a Rockies-like orography in the near future.

5. Acknowledgments

The authors are grateful to the Climate Dynamics Program of the United States National Science Foundation for supporting this research (Grant ATM-9024832). Computations were carried out on the Cray Y-MP computer at the National Center for Supercomputing Applications at the University of Illinois at Urbana-Champaign.

REFERENCES

Blackmon, M. L. 1976. A climatological spectral study of the 500 mb geopotential height of the Northern Hemisphere. *J. Atmos. Sci. 33*, 1607–1623.

Branstator, G. 1990. Low-frequency patterns induced by stationary waves. *J. Atmos. Sci. 47*, 629–648.

Cai, M. and Mak, M. 1990. Symbiotic relation between planetary and synoptic scale waves. *J. Atmos. Sci. 47*, 2953–2968.

Cai, M. and van den Dool, H. M. 1991. Low-frequency waves and traveling storm tracks. *J. Atmos. Sci. 48*, 1420–1436.

Hendon, H. H. 1986. The time-mean flow and variability in a nonlinear model of the atmosphere with orographic forcing. *J. Atmos. Sci. 43*, 433–448.

Karoly, D. J. 1990. The role of transient eddies in low-frequency zonal variations in the Southern Hemisphere circulation. *Tellus 42A*, 41–50.

Kidson, J. W. 1985. Index cycles in the Northern Hemisphere during the Global Weather Experiment. *Mon. Wea. Rev. 113*, 607–623.

Kidson, J. W. 1986. Index cycles in the Southern Hemisphere during the Global Weather experiment. *Mon. Wea. Rev. 114*, 1654–1663.

Kidson, J. W. 1988. Indices of the Southern Hemisphere zonal wind. *J. Climate 1*, 183–194.

Mo., K. C., Zimmerman, J. R., Kalnay, E. and Kanamitsu, M. 1991. A GCM study of the 1988 United States drought. *Mon. Wea. Rev. 119*, 1512–1532.

Qin, J. and Robinson, W. A. 1992. Barotropic dynamics of interactions between synoptic and low-frequency eddies. *J. Atmos. Sci. 49*, 71–79.

Roads, J. O. 1987a. Predictability in the extended range. *J. Atmos. Sci. 44*, 3495–3527.

Roads, J. O. 1987b. Estimate of errors in lagged time average numerical weather prediction. *Tellus 39A*, 492–499.

Robinson, W. A. 1991a. The dynamics of low-frequency variability in a simple model of the global atmosphere. *J. Atmos. Sci. 48*, 429–441.

Robinson, W. A. 1991b. The dynamics of the zonal index in a simple model of the atmosphere. *Tellus 43A*, 295–305.

Tribbia, J. J. and Baumhefner, D. P. 1988. Estimates of the predictability of low-frequency variability with a spectral general circulation model. *J. Atmos. Sci. 45*, 2306–2317.

Tung, K. K. and Rosenthal, A. J. 1986. On the extended-range predictability of large-scale quasi-stationary patterns in the atmosphere. *Tellus 38A*, 333–365.

Zangvil, A. 1981. Some aspects of the interpretation of spectra in meteorology. *Boundary-Layer Meteorology 21*, 39–46.